Published in Current Nanoscience 2, issue 4, 337-350, 2006
which should be used for any reference to this work

High Resolution Interference Microscopy: A Tool for Probing Optical Waves in the Far-Field on a Nanometric Length Scale

Carsten Rockstuhl*, Iwan Märki, Toralf Scharf, Martin Salt, Hans Peter Herzig and René Dändliker[#]

University of Neuchâtel, Institute of Microtechnology, Rue A.-L. Breguet 2, CH-2000 Neuchâtel, Switzerland

Abstract: High Resolution Interference Microscopy (HRIM) is a technique that allows the characterization of amplitude and phase of electromagnetic wave-fields in the far-field with a spatial accuracy that corresponds to a few nanometers in the object plane. Emphasis is put on the precise determination of topological features in the wave-field, called phase singularities or vortices, which are spatial points within the electromagnetic wave at which the amplitude is zero and the phase is hence not determined. An experimental tool working in transmission with a resolution of *20 nm* in the object plane is presented and its application to the optical characterization of various single and periodic nanostructures such as trenches, gratings, microlenses and computer generated holograms is discussed. The conditions for the appearance of phase singularities are theoretically and experimentally outlined and it is shown how dislocation pairs can be used to determine unknown parameters from an object. Their corresponding applications to metrology or in optical data storage systems are analyzed. In addition, rigorous diffraction theory is used in all cases to simulate the interaction of light with the nano-optical structures to provide theoretical confirmation of the experimental results.

Keywords: Interferometry, Nano-optic, Super resolution, Diffraction.

1. INTRODUCTION

To obtain structural information about objects by using light, various parameters that characterize the optical wave-field can be used as the carrier of information. The underlying idea is generally that upon illuminating the object with a well defined wave-field, the parameters that characterize the wave-field are measured after interaction with the sample and a change of those parameters permits the reconstruction of either geometrical or optical information about the object.

Widely used as an information carrier is obviously the amplitude or intensity distribution of a wave-field [1]. But also the state of polarization of the reflected light [2], the particular wavelength of light scattered e.g. resonantly on small metallic nano particles [3], or the spatially localized generation of light with higher frequencies employing nonlinear effects [4] can be used to obtain information about the structure under investigation. All those methods rely on the detection of field components scattered by the objects into the far-field. Hence, information contained in evanescent field components that do not carry energy is lost and the corresponding reconstruction of object information is subject to an incertitude for object sizes smaller than approximately half the wavelength. Overcoming this limit, known as the Abbe-criteria, is currently the subject of investigations with various approaches. The most direct way to collect information in addition to the far-field (herein defined as the spatial domain far away from the sample, as compared to the wavelength, where the amplitude of evanescent waves is negligible) is to obtain information about the near-field (defined as the spatial domain close to the sample, as compared to the wavelength, where the evanescent waves have finite amplitudes). It is possible by employing techniques that detect the field-distribution close to the sample. This can be done by e.g. scanning the field directly above the sample with a small aperture (Scanning Near-field Optical Microscope (SNOM), where the resolution is given to a first approximation by the diameter of the opening aperture) [5], or using a small probe that scatters light into the far-field and transfers evanescent into propagating wave-components (scattering-SNOM), where the resolution is given to a first approximation by the size of the scattering object [6]. However, the drawback of those methods is their scanning character, which prevents the collection of information about the entire sample in parallel. In addition, the distance between sample and probe has to be kept constant with a high precision in the *nm* range, a limitation that puts lower bounds on the overall information acquisition time.

The phase of an optical wave-field is an additional parameter that can be used to obtain structural information about phase objects. Phase objects are characterized by a phase only transmittance function, hence the absorption of light and the corresponding direct modulation of the transmitted amplitude is excluded. If the phase variation ratio of the scattered to the directly transmitted light (zero diffraction order) is small compared to unity, the phase modulation can be directly transferred into an intensity modulation by phase shifting the light diffracted into the zero order by a quarter wavelength [7]. This is called Zernicke phase contrast method.

If the phase modulation gets larger this method can no longer be used directly. In such a strong interaction domain,

*Address correspondence to this author at the Institute for Solid State Theory and Optics, Friedrich-Schiller University Jena, Max-Wien Platz1, D-07743 Jena, Germany; Tel: 0049 (0) 3641 947 174; Fax: 0049 (0) 3641 947 177; E-mail: Carsten.Rockstuhl@Uni-Jena.de

[#]At the time the work presented in this review was carried out, all the authors were with the University of Neuchâtel, Switzerland. C. Rockstuhl is now with the Friedrich Schiller University in Jena, Germany and Martin Salt is with Heptagon Oy., Switzerland.

the scattered wave-field no longer behaves smoothly and turbulence in the phase field will appear. If the strength of the scattered field is sufficient to interfere completely destructively with the zero-order, spatial points in the wave-field exist, where the amplitude is zero. Associated with this zero amplitude is a phase singularity, a spatial point at which the phase ϕ is not determined, as it is defined as $\tan(\phi) = \frac{\mathrm{Imag}(E)}{\mathrm{Real}(E)}$ with E being a scalar wave-field component. Phase singularities were first observed in a seminal work by Nye and Berry [8]. As a general classification of phase singularities, one distinguishes between screw and edge singularities (also called dislocations or optical vortices). The simulated phase distribution of an idealized screw singularity, as shown in Fig. **1(a)**, is characterized by a point in which the amplitude is zero and the phase varies along a circle in the close vicinity of the singularity by a multiple m of 2π, with m being the topological charge or strength of the singularity [9, 10]. A positive sign of the charge denotes a right-handed screw of the phase front in the propagation direction; a negative sign denotes a left-handed screw. The phase in Fig. **1(a)** is shown in a plane perpendicular to the propagation direction. Along the propagation direction of the laser beam, such a singularity produces a line with an intensity equal to zero. The simulated phase distribution of an ideal edge dislocation, as shown in Fig. **1(b)**, corresponds to a line of zero intensity transverse to the propagation direction. The phase has a phase jump of exactly π across this line. In a cut trough any one of the two transversal coordinates and the longitudinal coordinate, the phase distribution resembles the distribution of a screw singularity: it appears as a point in which the amplitude is zero and a phase varies along a closed circle around the singularity by 2π.

These phase singularities appear manifold in nature, with laser beams of Gauss- Hermite type (edge singularities) and Gauss-Laguerre type (screw singularities) being the most prominent examples [11]. Screw dislocations have also been observed in random speckle wave-fields [12, 13]. They can be generated in a controlled manner by employing laser resonators [14], appropriately designed phase plates [15, 16], mode converters [17] or computer generated holograms [18, 19], and they can be used in a range of applications, e.g. for the trapping of particles [20] or atoms [21].

The application of phase singularities in conjunction with a high resolution interference microscope in order to characterize objects with a precision much smaller than the wavelength was first proposed in a series of pioneering publications at end of the eighties by Tychinsky and co-workers [22-24]. The basic idea of this approach is shown in Fig. (**2**) [25]. Consider an object on the surface of a substrate illuminated with a plane wave from above. In the present example the object is a trench with a width of $w = 300\ nm$, a height of $h = 488\ nm$ and of infinite extent in the third direction, made in a substrate with $n = 1.5$. The wave is TM polarized and the vector of the magnetic field oscillates parallel to the space invariant direction of the structure. The wavelength is $\lambda = 488\ nm$. The figure shows the grey-scale intensity distribution with white being high intensity and dark being low intensity. The iso-phases are also shown. A phase singularity of edge type, marked by the two white circles, appears directly behind the trench as a result of the interference between the unperturbed transmitted wave-field (zero order) and the scattered field by the object. The field distribution was calculated with the Rigorous-Coupled-Wave-Analysis [26, 27], a numerical tool that solves

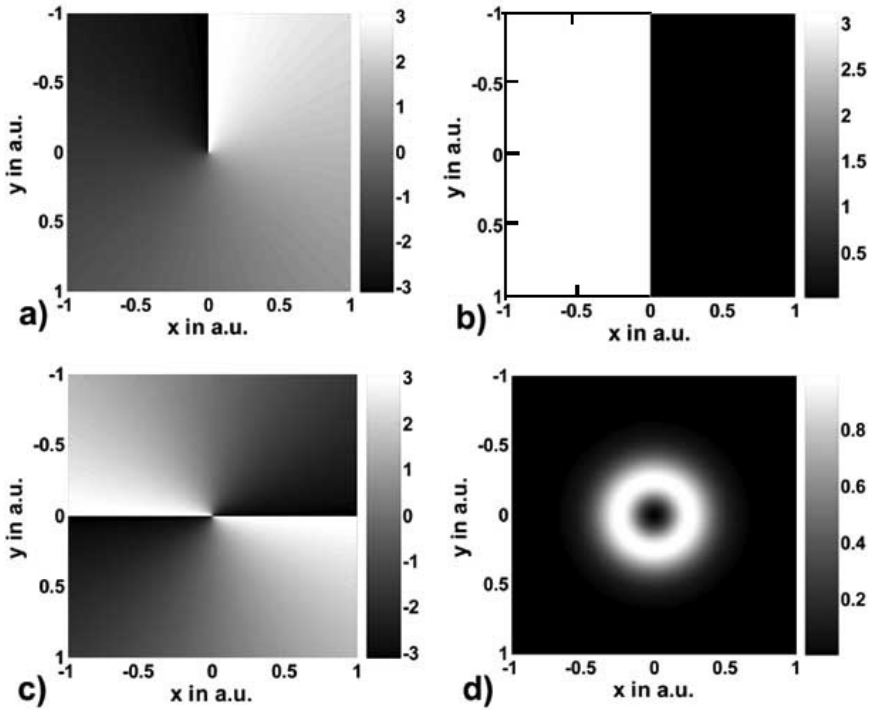

Fig. (1). In-plane phase distribution of (**a**) a screw-type singularity and (**b**) an edge-type singularity.

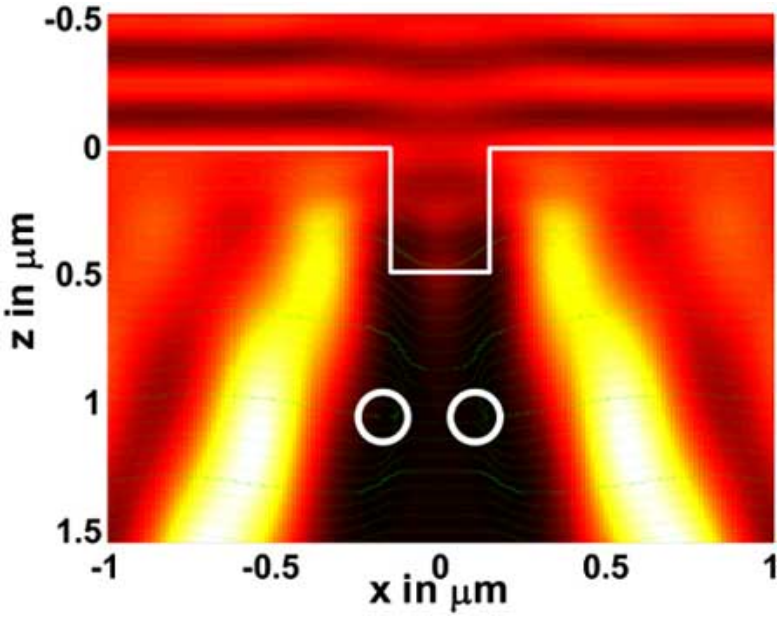

Fig. (2). Basic geometry of a non-periodic scattering object that causes the generation of an edge dislocation in the transmitted wave-field due to complete destructive interference of the scattered field with the incident field. The simulated intensity and isophases of the wave field are shown, the circles denote the position of the singularities and the details of the structure are outlined in the text.

Maxwell's equations rigorously, employing periodic boundary conditions. Nevertheless, this approach can be applied likewise to aperiodic objects under certain constraints for the periodicity (the period in the simulation has to be much larger than the transverse extension of the object and the period should not be an integer multiple of the illuminating wavelength [25, 28]). The field distribution shown is filtered such that waves with spatial frequencies of $|k_x| > k_0$ (e.g. evanescent waves) are not shown and the amplitude and phase distribution is hence accessible by means of interferometric equipment in the far-field. It can be seen that directly behind the structure a pair of phase singularities appears whose separation can be related to the width of the structure. Because the singularities are mathematically exact points, measuring their distance is only subject to technical limitations and super-resolution is generally possible. However, this super-resolution does not refer to a physical object but only to the particular topological feature in the wave-field. As the size of the objects are also comparable to the wavelength, scalar theory can no longer be used to describe the interaction of light with those objects properly, and rigorous numerical tools have to be used for the exact simulation of the light interaction. It turns out, that a direct relation between object properties and the singularities does not exist and only the use of *a priori* knowledge about the structure (like height, profile parameters, refractive index) allows to reconstruct the unknown object parameters [29, 30, 31-33]. The question whether true super-resolution of objects smaller than half the wavelength is obtainable remains an open issue.

In this mini-review, we will report on our latest results in the field of High-Resolution Interference Microscopy (HRIM) using an instrument that works in transmission. This article is written with the intention to give an overview of the potential of HRIM to a broader audience. The paper is structured as follows. In section 2 we will present the experimental set-up of the instrument. Results of the analysis of screw dislocation generated by Computer Generated Holograms (CGH) are presented in section 3. In section 4 edge singularities generated by periodic elements and in section 5 by single elements are analyzed. In both sections the conditions for the appearance of singularities are outlined and it is shown that super-resolution of objects is not possible. To obtain singularities in the far-field, the object has to have a certain width (at an optimum phase depth) that is comparable with the Abbe-resolution limit. However, once phase singularities appear, their position can be determined with a theoretically unlimited resolution. This property favors their use in applications such as metrology or optical data storage systems.

2. Experiemental Set-Up

The experimental set-up of the interferometer is shown in Fig. **3(a)**. A photograph of the actual instrument is shown in Fig. **3(b)**. The light source in the experiments is either an Argon laser ($\lambda = 488\ nm$) or a HeNe laser ($\lambda = 632.8\ nm$) coupled to a monomode fiber. A fiber coupler splits the wave-field into a reference and an object arm with an adjustable energy ratio. This permits to optimize the contrast of the interference fringes for an easier determination of the phase. In the object arm, the light that exits the fiber illuminates the sample mounted on a high precision piezo stage, which allows positioning in the x and y direction with an accuracy of *10 nm* and in the z-direction with an accuracy of *1 nm*. The light from the exit of the fiber is collimated onto the object such that the illuminating wave sufficiently resembles a plane wave (its Gaussian waist is much larger than the transversal extension of the object). The transmitted light enters a standard microscope, which consists of a telescopic system with the first lens being a variable objective and the second lens having a fixed focal length of *250 mm*. The first objective basically limits the angular

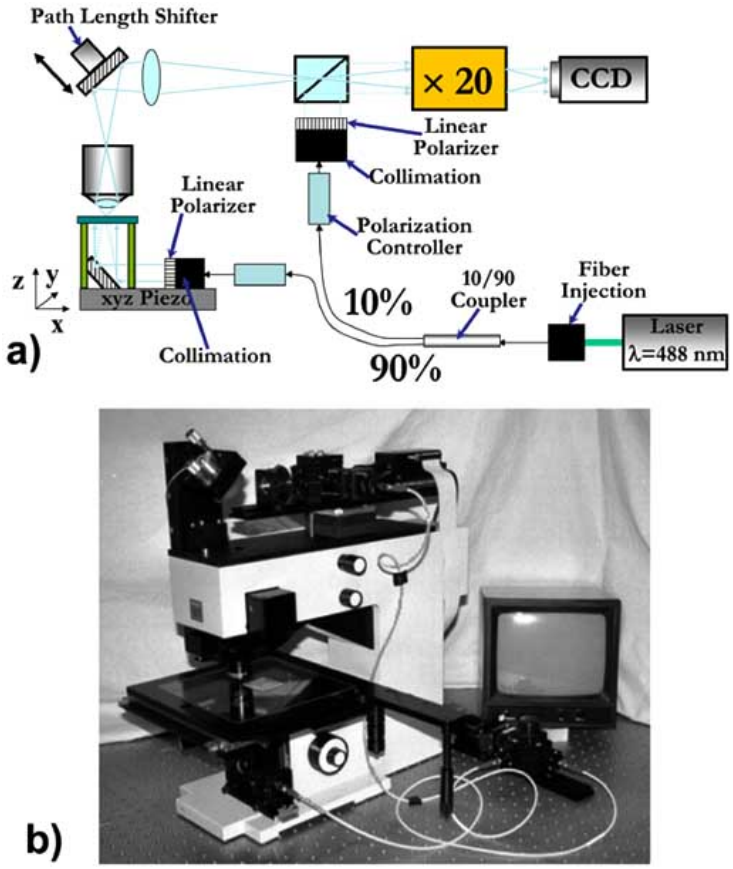

Fig. (3). Experimental scheme of the High-Resolution Mach-Zehnder interferometer used in the experiments in (**a**) and a photograph of the actual instrument in (**b**).

spectrum transmitted by the optical system. A high numerical aperture (*N.A.*) ensures generally a high resolution. In most of the measurements we have used a *50 x* objective with a *N.A. = 0.85*. For the measurements with the CGHs the first magnification stage has to be limited in its power, because the diffraction orders have to be separated and selected in an intermediate plane. In these experiments the objective of the first magnification stage was a *10 x* objective with a *N.A. = 0.2*. The second magnification stage for obtaining superhigh-resolution is again a telescopic setup with the first lens being a *50 x* objective and the subsequent lens having a focal length of $f = 200\ mm$. This second magnification stage acts on both reference and object arm, as the two beams interfere before entering the second magnification stage. The resulting intensity distribution is imaged onto an 8-bit CCD camera. The overall magnification of the instrument is usually calibrated with the help of a grating of precisely known period as reference object. The phase distribution of the wave-field in the object arm is obtained employing a classical 5-frame algorithm, where 5 frames of the 2-D intensity pattern are recorded, each frame being shifted in phase by adding an additional phase of $\lambda/4$ with the help of the piezo-mounted mirror in the object arm [34].

For measuring the intensity and phase distribution of screw singularities, recording the phase distribution at a single z-position is sufficient, because the dislocation can be fully observed in the x-y-plane. For the recording of dislocations of the edge type, as shown in Fig. (**1**), a three-dimensional scan of the field distribution has to be carried out, because it is most unlikely that the first selected plane of observation corresponds exactly to the plane where the singularity is located. Hence, the usual procedure consists of firstly recording the intensity and phase in a certain x-y-plane at z_0. Subsequently, to move the piezo stage automatically by a distance Δz to translates the object plane by a specified distance, and then to record intensity and phase for this plane. For an unambiguous reconstruction of the entire phase distribution in the 3D space, the step distance has to be significantly smaller than the wavelength. Usually a value of $\Delta z = 50\ nm$ was used. However, this value also limits the resolution of the position of the singularities in the z-direction, hence the step distance was occasionally reduced to *10 nm* to improve resolution. This is of course only a technical limitation and does not represent any fundamental limit. The resolution in the x-y plane is classically given by the demagnified size of the pixels from the camera plane to the object plane. Wave-fields with a resolution down to *20 nm* have been measured [33, 35].

3. Screw Dislocations

The screw dislocations analyzed in this work [36] were generated in the various diffraction orders of a CGH that was designed for producing a Gauss-Laguerre beam *GLpm* with the orders $p = 0$ and $m = 1$ in the first diffraction order off-axis, abbreviated as GL01 [11]. p is the radial mode

parameter of the GL beam and m the azimuthal mode parameter. Following the standard procedure for the design [37] the pattern of the CGH was obtained by computer as the result of the interference of a GL beam of the desired order and waist with a plane reference wave that propagates under a certain angle with respect to the GL beam. After an appropriate clipping procedure, the CGH becomes a binary grating with a period Λ that posses the proper phase transmittance function for generating a singularity of charge *1*. The sinus of the angle θ under which the various diffraction orders propagate in space is given by an integer multiple of λ/Λ. The holograms were printed using a photocomposer and subsequently reduced in a photolithographic process by a factor of 10 and then imaged on a substrate covered with photoresist [38]. After development, the sample is used as a phase-only object that works in transmission. We have chosen for the underlying binary grating a period of $10\ \mu m$ and the depth of the gratings was evaluated by means of an atomic force microscope to be *600 nm*.

Figure **4(a)** shows the measured intensity distribution and Fig. **4(b)** shows the corresponding phase distribution in the first diffraction order of the CGH upon illumination with a plane wave. Again, white denotes high intensity and dark denotes low intensity. For the phase distributions, black corresponds to a phase level of $-\pi$ and white denotes a level of π. To select the desired single diffraction order, an aperture stop was positioned in an intermediate plane within the first magnification stage where the various orders appeared spatially well separated. The measured intensity distribution has the well-known doughnut shape and the phase distribution shows the expected characteristics of a screw singularity with charge *1*. The position of the origin of the singularity can be identified with a spatial resolution that corresponds to about three pixels of the CCD camera. This is a significant advantage compared with the established experimental technique of fork-interferometry, where the laser beam under investigation interferes with a smooth reference wave at a specific angle [39]. The regular fringe pattern of straight lines shows at the position of the singularity a bifurcation. However, the spatial resolution of this direct method is limited by the period of the interference fringes, given by the angle between the two interfering waves. Values in the order of tens of micrometers are usually obtained. Incoherent background light makes it impossible to denote unambiguously the position of the lowest intensity and the results are rather smeared out over an extended domain. Compared with measuring the intensity distribution only, the advantage of the phase measurement relies on the suppression of this background light. The resolution of our phase image in the vicinity of the singularity is limited by the number of discretization levels of the recorded intensity images of the CCD camera. The gain of the CCD was adjusted such that the peak of the intensity did not cause saturation. Hence, low intensity values close to the singularity are clipped to a single value if their difference is below one discretization level. This results in the measurement of spatially extended domains with the same intensity, whereas the genuine intensity distribution will show slight variations. An increase of the gain for using the entire dynamic range in the vicinity of the singularity or the use of a CCD camera with a higher dynamic range would improve this restriction of the resolution. Nevertheless, these reasons for the limitation of the position of the singularity are exclusively of technical nature and do not represent a fundamental restriction. The slight spiral-like distortion of the phase distribution seen in Fig. (**4**) originates from a sub-optimal adjustment of the radius of curvature of the phase front between the object and the reference arm.

Having an instrument with such a superior resolution, an interesting question to address was whether dislocations with a charge of *2* generated by such an optical element are genuinely higher order dislocations or whether they will split into two singularities of unity charge, which are closely spaced but still separated. To get such a phase object, the second diffraction order of the CGH was used, as the additional phase delay in this order of the transmitted wave-field corresponds exactly to one wavelength. The measured intensity and phase distribution are shown in Fig. **5(a)** and **(b)**, respectively. The intensity again shows the typical ring-shaped distribution with an intensity zero in the center of the beam that is more extended in space, corresponding to a higher order Gauss-Laguerre beam, i.e. *GL02*. Nevertheless, the phase distribution shown in Fig. **5(b)** clearly reveals the

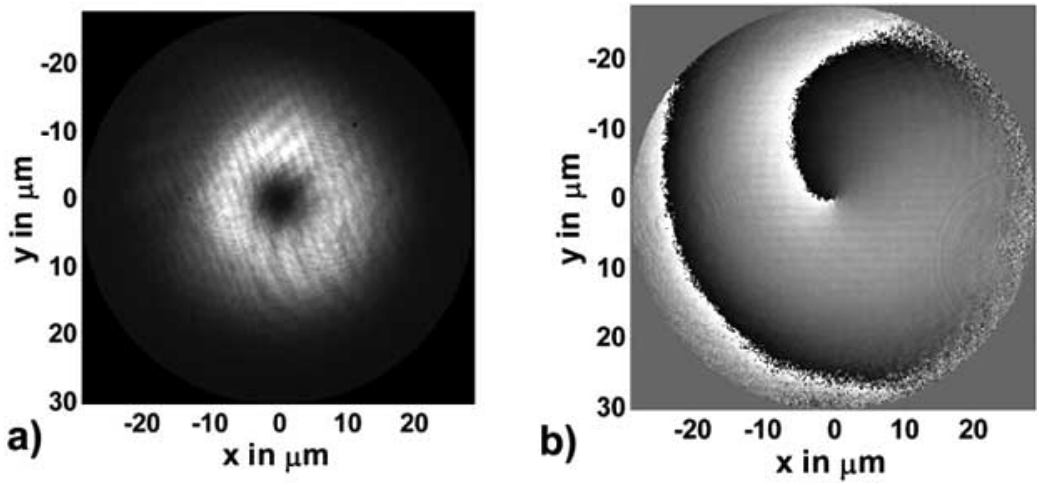

Fig. (4). (**a**) Measured intensity distribution and (**b**) phase distribution of a screwtype dislocation of charge *1* generated by a CGH.

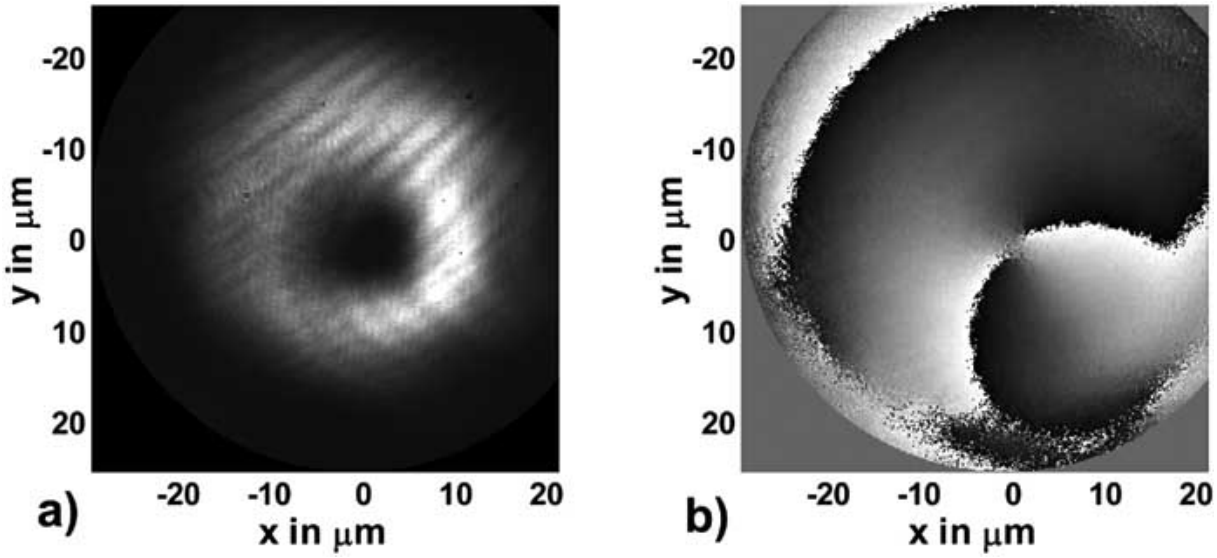

Fig. (5). (**a**) Measured intensity distribution and (**b**) phase distribution of a screwtype dislocation of charge *2* generated by a CGH.

existence of two closely spaced but well distinguishable singularities of charge unity. Their spatial separation in the object plane is *2.5 μm*. The splitting is explained by analyzing the modal composition of the laser beam in terms of Gauss-Laguerre modes. The major mode content of the beam corresponds obviously as outlined before to a *GL02*. But a slight off-set by a *GL00* mode propagates likewise in the second diffraction order which adds coherently as a background and destroys the point of zero amplitude in the center of the beam and splits it into two points that have the same distance from the optical axis of the beam. The singularity of charge $m = 2$ splits into two singularities with unity charge. Three main contributions for the generation of this parasitic fundamental mode are identified. Firstly, the CGH was designed to generate a *GL01* beam; hence the amplitude transmittance function of the CGH was adapted for creating the amplitude distribution of this mode. However, as the amplitude distribution of higher order GL modes slightly deviates, those beams cannot be generated by the same CGH precisely. Other modes will have minor contributions in the power spectrum of the modal composition of the laser beam and those modes will destroy the perfect shape of the GL02 mode. Secondly, the clipping procedure in the transmission function onto a binary transmission function introduces errors, which cause the generation of other modes. And thirdly, the sub-optimal height profile due to fabrication tolerances of the phase structure used for the CGH degrades the diffraction efficiency and promotes further the generation of higher order Gauss-Laguerre modes as well as the fundamental mode. Whereas the first reason is a parasitic effect that could be overcome by using properly designed CGHs, the remaining two reasons are more fundamental. A CGH that generates a *GL02* mode in the first diffraction order was likewise employed, but similar results were obtained [36]. In none of the cases a genuine singularity of higher charge was observed within the accuracy of the measurements, as it always split into multiple singularities with a unity charge. Overall, Gauss-Laguerre modes with an azimuthal mode parameter up to $m = 4$ were investigated.

By employing this HRIM the concept of higher order singularities generated by CGHs was analyzed and it was shown that the intensity distribution also looks in the most cases just like a higher order Gauss-Laguerre beam with multiple singularities, they never coincide precisely but always split.

4. Edge Dislocations Generated by Periodic Objects

The other type of singularity, the edge dislocation, was likewise investigated with the HRIM by employing various structures. A simple object that helps to understand the condition for the appearance of an edge singularity is a periodic structure, a grating. The transmitted field of a grating illuminated under normal incidence is given as a superposition of an infinite number of plane waves that propagate under an angle θ_m. The angles are given by the grating law $\sin(\theta_m) = m\frac{\lambda}{\Lambda}$, with m being the diffraction order, Λ the period and λ the illuminating wavelength. The complex amplitude of each of the transmitted plane waves depends on the distribution of dielectric material within each period. If the period is much larger than the wavelength, the amplitudes are calculated with the thin-element approach (TEA) as the Fourier-Transformation of the transmittance function of a single period. If the period gets comparable to the wavelength, the approximations in the TEA are no longer valid and rigorous diffraction theory has to be used for determining the amplitudes correctly [26, 27]. The number of plane waves that will contribute to the image formation depends on the numerical aperture (*N.A.*) of the optical system. Only orders with $N.A. > \sin(\theta_m)$ are measurable in the far-field, hence the entire field can be decomposed into a finite number of plane waves with amplitudes a_m. For the appearance of a singularity in the far-field, there must be a point in space where the complex amplitude of the super-positioned plane waves goes to zero. This is only possible in the far-field of a grating if the strongest amplitude a_n is

smaller than the sum of all the other amplitudes [40]. Hence the condition reads as

$$\Sigma_{m\neq n}\left|a_m\right| \geq \left|a_n\right| \qquad \forall n\,. \qquad (1)$$

For measuring singularities with the HRIM at least the zero and first diffraction orders have to propagate through the optical system, which corresponds to the resolution criteria as formulated by Ernst Abbe.

For the experimental investigations various gratings were used, either binary gratings in SiO_2 or phase gratings with a continuous profile in photoresist. A SEM image of such a grating with a continuous profile, written by two-beam interference, is shown in Fig. (**6**). From such an image all the necessary geometrical parameters of the grating can be obtained, such as height, period and surface profile. The measured phase distribution (iso-phases) in the far-field of this particular grating is shown in Fig. **7(a)** and the simulated phase distribution is shown in (**b**). The wavelength of the laser in this experiment was $\lambda = 0.633\ \mu m$ and the numerical aperture of the objective was *N.A. = 0.85*. The different z-scale in measurement and simulation are observed as it was not possible to determine the exact spatial origin of the measurement with respect to the surface of the grating, whereas in the simulation the absolute distance to the surface is shown in the z-axis. As the structure is invariant in the y-direction, the phase distribution is likewise invariant in this direction. In the measurement we can take advantage of the massive parallel data acquisition by the CCD camera and for suppressing effectively the always present phase noise, the measured phase distribution was averaged over a certain number of lines of the CCD camera in y-direction.

First of all we can see in Fig. (**7**) that the periodic transmittance function generates a periodic wave-field in the

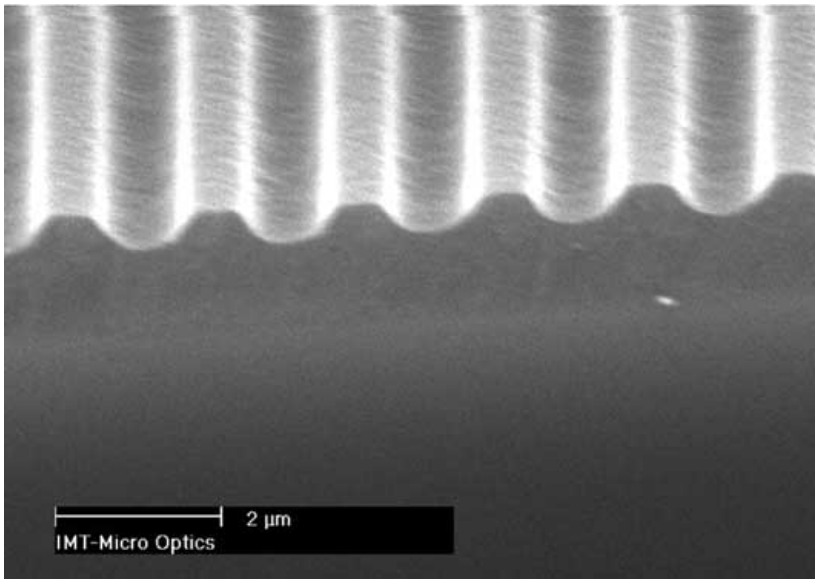

Fig. (6). SEM image of a surface grating written by two-beam interference lithography in a PMMA photoresist.

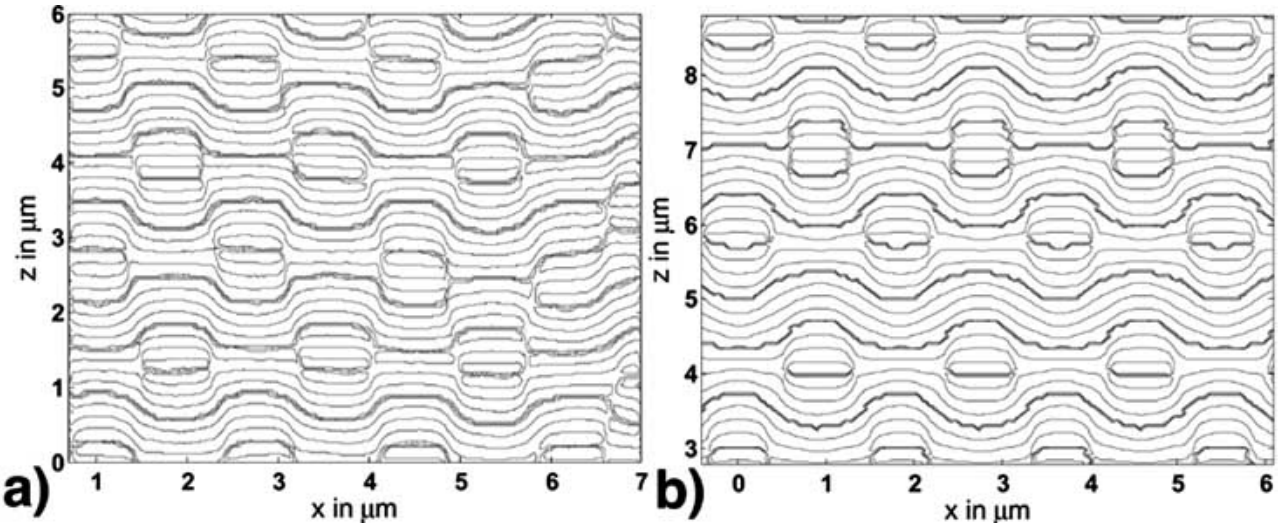

Fig. (7). (**a**) Measured phase distribution generated by the surface grating in transmission and (**b**) simulated phase distribution in the far-field generated by the surface grating in b. The grating is characterized, as deduced from the SEM image, by a *period* of $\Lambda = 1.833\ \mu m$, $h = 0.65\ \mu m$ and a surface profile as given in the text. The illuminating wave-field is a TE-polarized plane wave with $\lambda = 0.633\ \mu m$.

transverse x-direction with phase singularities being an ideal indication for determining exactly the period. As the period can be likewise obtained with high accuracy from the measurement of the propagation direction of the various diffraction orders, the field distribution of such a grating can be applied for calibrating exactly the object size that a single pixel of the CCD camera represents. The dislocations can be seen in the points where all isophases unite or emerge, respectively. They are of edge-type. At a certain propagation distance z_0 where the dislocation is situated a line plot in x-direction of the phase distribution would correspond to a periodic alternation of sharp phase jumps by π. The measured and the simulated phase distribution show excellent agreement. The slight deviation of the measured phase distribution reveals the signature of a local perturbation of the grating, probably due to a dust particle on the surface that acts as an additional scatterer. The measurement of this feature is not reproducible, as the relocalization of exactly the same point of the grating is not possible, whereas the general field distribution can be repetitively measured. A richer variety of topological features can be obtained by measuring gratings with a larger period, as more diffraction orders will contribute to the wave-field. The measurement of the phase distribution permits principally the reconstruction of the surface profile. This can be done first of all by optimizing the complex amplitudes of a discrete number of plane waves, the number of which corresponds to the number of diffraction orders generated by a specific period and transmitted by the optical system, such that the generated singularities correspond to the spatially coordinates of the measured singularities. Subsequently the surface profile has to be determined that generates exactly this set of amplitudes. Unfortunately, to the best of the author's knowledge no inverse rigorous diffraction theory exist, which would permit such a direct reconstruction. Additionally, the problem most likely does not have a unique solution and various gratings exist that generate the same set of diffraction amplitudes. This makes it necessary to use *a priori* knowledge about the structure to determine the proper profile. Nevertheless, as we will show below for non-periodic objects, if such additional information is available, parameters of the structure can be revealed with high accuracy based on the measured positions of singularities.

5. EDGE DISLOCATIONS GENERATED BY APERIODIC OBJECTS

Edge dislocations can also be generated by single / non-periodic objects if the interference of the scattered with the incident field is completely destructive at a specific spatial point. The angular spectrum of the scattered field is not discrete as in the case of periodic objects, but continuous. Hence, for a mathematical derivation of the condition for the appearance of dislocations in the far-field we extend the condition given in the last section to the limit of an infinite period, which reads as [25]

$$\int_{\nu_{N.A.}} \left|a(\nu)\right|(1-\delta(\nu-\nu_0))d\nu \geq \int_{\nu_{N.A.}} \left|a(\nu)\right|\delta(\nu-\nu_0)d\nu \quad (2)$$

with $a(\nu)$ being the Fourier-coefficient of the transmittance function at the spatial frequency ν, ν_0 the spatial frequency of the zero order direct transmitted light and with the amplitude spectrum integrated over all spatial frequencies that will be transmitted by the optical system. In the thin-element approach and employing scalar diffraction theory, the transmittance function $T(x)$ relates the incident field $F_{Inc}(x)$ and the transmitted field $F_{Trans}(x)$ linearly *via* $F_{Trans}(x) = T(x)F_{Inc}(x)$.

5.1 Phase Singularities Produced by Phase Bars

The condition is general and can be used to determine whether an arbitrary object is capable of generating a phase singularity in the far-field. With respect to an experimental situation we have investigated in detail the conditions for the appearance of a singularity for a phase bar surrounded by air. Its transmittance function is given by

$$T(x) = \begin{cases} e^{i\frac{2\pi h}{\lambda}(n-1)} & |x| \leq \frac{w}{2} \\ 1 & |x| > \frac{w}{2} \end{cases} \quad (3)$$

The phase bar is characterized by a width w, a height h and a refractive index n and the induced phase delay of the wave-field inside the bar is given by $\Delta\phi = \frac{2\pi h}{\lambda}(n-1)$. Inserting this transmittance function into Eq. 2 will give the particular condition of

$$0 = -1 + \frac{4}{\pi}\sin\left(\frac{\Delta\phi}{2}\right)\int_0^{\pi w} \frac{\left|\sin\left(\frac{t}{\lambda}\right)\right|}{t}dt \quad (4)$$

that has to be fulfilled for a certain phase bar in order to generate a singularity. The integral is taken over all propagating orders with a spatial frequency of $|k_x| < k_0$. This corresponds to the condition of a $N.A. = 1$. The unity term is the zero-order transmission and the second term expresses the scattered field of the structure. By taking an optimal phase delay of $\Delta\phi = \pi$ the equation is evaluated in Fig. (**8**). It shows the lowest amplitude value in the transmitted wave-field and the right hand side of Eq. 4 evaluated as a function of the width of the phase bar. It can be seen that the appearance of the singularity predicted by Eq. 4 and the amplitude zero in the transmitted wave-field coincide as expected. For a zero width no scattered field is generated at all and the transmitted field consists of a plane wave. Increasing the width generates scattered field but its amplitude is not sufficient for completely destructive interference with the zero-order. Nevertheless, a steady increase in size causes an increase of the strength of the amplitude and at a width of $\approx \lambda/4$ a dislocation appears. This size is comparable to the classical resolution limit and as a consequence phase singularities cannot be employed for obtaining super-resolution in a classical sense. The width at which a singularity is generated also depends on the phase delay induced by the phase bar. For an induced phase delay of $\Delta\phi = 2/3\ \pi$, the width of the phase bar has to be $\approx 0.3\ \lambda$

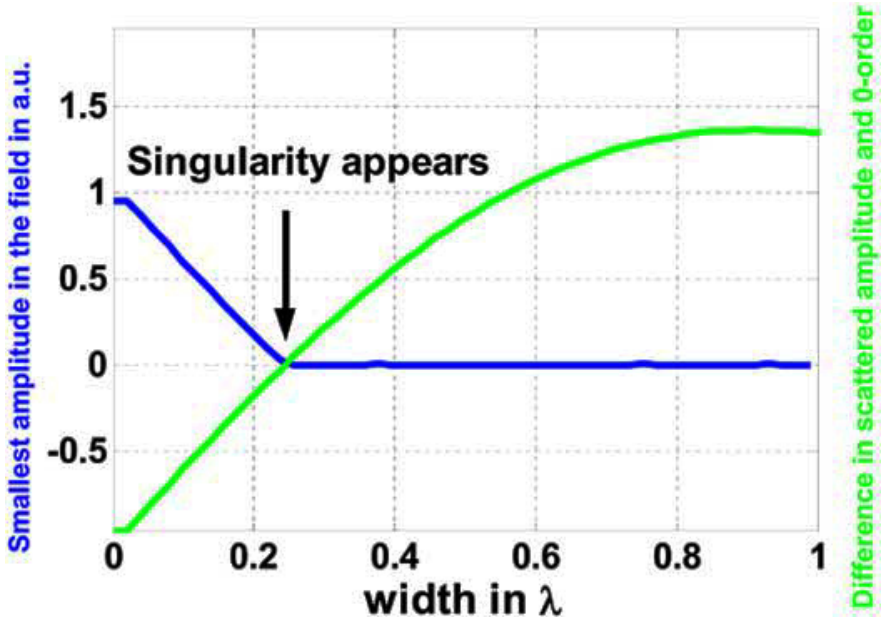

Fig. (8). Analyzing the necessary width of a phase object that generates a phase singularity in the far-field as a function of the induced phase delay by calculating the smallest amplitude appearing in the wave-field behind a phase bar and numerical evaluation of the inequality of Eqn. 2.

and a width of ≈ 0.6 λ is necessary at a phase delay of $\Delta\phi = 1/3\ \pi$.

The value obtained via this scalar theory can in each case only be used as a first indication whether a structure generates a dislocation or not, as the size of the scatterer compared to the wavelength no longer justifies the approximation made in scalar theory. A rigorous solution of Maxwell's equations has to be used instead. Fig. (**9**) shows the separation between a pair of singularities behind a trench calculated with the Rigorous-Coupled-Wave-Analysis [26, 27]. The geometrical situation corresponds to the case shown in Fig. (**2**). The trench is made in a material with $n = 1.5$, it has a height of $h = 488\ nm$ and it is illuminated with a plane TM-polarized wave with $\lambda = 488\ nm$. For the determination of the separation, the transmitted field distribution in space was calculated by assuming $N.A. = 1$ and points in the field with the highest phase gradient were evaluated. This explains why points appear in Fig. (**9**) even for a width of the scatterer smaller than the critical width for generating dislocations. But it shows how those points with the highest phase gradient get closer. When they coincide, the singularity is born, as indicated by the arrow. A width of *170 nm* is necessary, which is somewhat larger than the value of *120 nm* as predicted by scalar theory. After a sudden increase

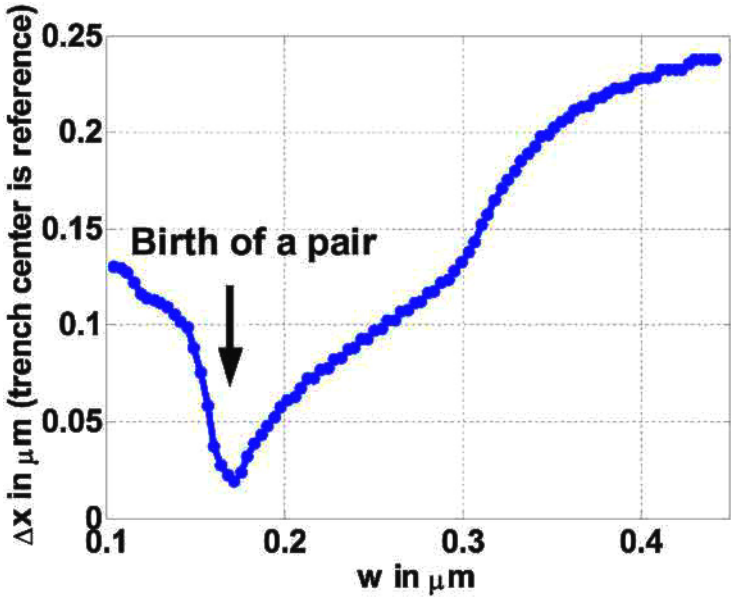

Fig. (9). Distance between pairwise generated singularities behind a trench as a function of its width as calculated with rigorous diffraction theory.

of the separation for widths slightly larger than the critical one, the distance grows fairly linearly with the width of the structure. Since the spatial position of the singularities can be evaluated with high resolution, this response allows also to determine the width of the scatterer with high accuracy if the other parameters are known.

A remark must be made on the choice of the TM polarization, which was selected specifically for this geometry of a trench. Singularities are generated at smaller feature sizes for TM polarization compared with the orthogonal TE polarization. This can be explained by considering the trench as an air wave guide surrounded by a high index material [41]. If the material would be a perfect conductor, a cut-off width would exist for TE polarization under which no mode can propagate within the structure. The same holds principally for high-index dielectric materials. The structure illuminated with this polarization will not generate sufficient scattered light to suppress the incident field in a specific spatial point. Such a limitation does not hold for TM polarization, where at least one mode always propagates in the structure. If a mode is excited within the structure, it propagates with a different propagation constant than the field in the surrounding medium. It accumulates a phase delay and once the field exists the structure, it interferes destructively if the phase delay is sufficient that will cause ultimately the generation of the singularity. For the opposite geometrical case, a phase bar on top of a substrate, TE polarized light generates a singularity at smaller object sizes, since the propagation constant of the TE polarized mode is always larger than that for the TM mode. A larger phase delay is accumulated by the light propagating in the dielectric wave guide and destructive interference is more pronounced.

Those predictions have also been recently verified experimentally [33] and as an example a measured phase distribution of a phase trench is shown in Fig. (**10**). The figure shows the measured intensity and phase distribution generated behind a trench in photoresist with a width and height of approximately *450 nm*. The illuminating wave propagating in the positive z-direction was TM-polarized with a wavelength of $\lambda = 488\ nm$. Results of the simulation of the experimental situation are shown in Fig. (**11**). Again excellent agreement between theory and experiment is found. The two small circles denote as a guide to the eye the position of the singularity pair whose separation can be directly related to the width of the trench. In the simulation, the surface of the structure is likewise shown, but the field inside the structure and in the region with $z < 0$ is not the true one, but only the back propagated transmitted field. The reflected field is not accessible with this set-up. Interesting to note that the generation of singularities in this back propagated field is at approximately $z = -1\ \mu m$ in the simulation. The different z-range in simulation and experiment is because it is not possible to define an absolute plane of reference in the z-scan with respect to the surface of the sample. The separation between the singularities, which can be directly related to the width of the trench, was evaluated for a series of samples and results are shown in Fig. (**12**). The difference in trench width for two subsequent samples amounts to between *20 nm* and *30 nm* and the maximum trench width was *500 nm* for sample 12. The smallest structure from our samples that could generate a phase singularity had a width of *360 nm* (sample 5). No singularities were observed from smaller structures. This width is larger than the rigorously predicted width, which is mainly due to the smaller aperture of the experimental equipment. With exception of the higher absolute width of the structure, necessary for generating a singularity, the qualitative behavior follows the theoretical predictions very closely. It can be seen that after a sudden increase in their distance shortly after the birth of the dislocation, their distance grows nearly linearly with the width of the structure.

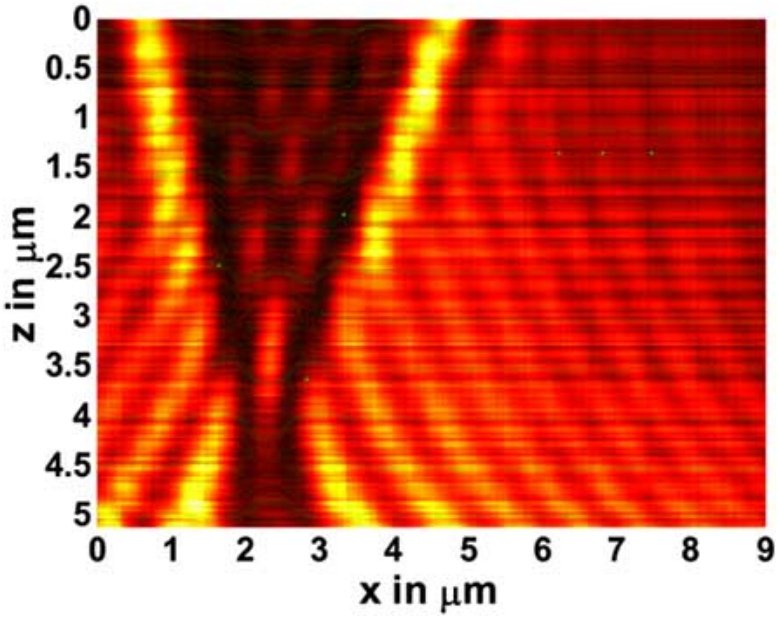

Fig. (10). Measured intensity and phase distribution generated by a trench that has a width of approximately *450 nm*.

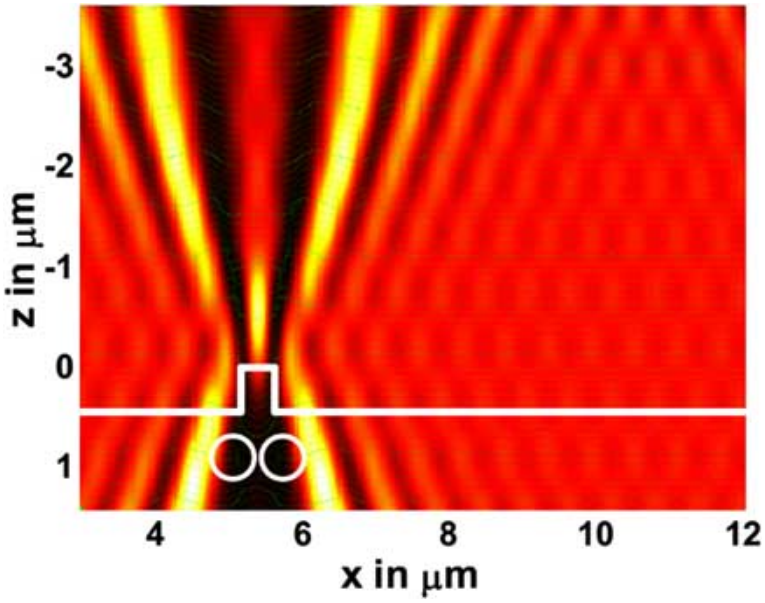

Fig. (11). Simulated intensity and phase distribution for comparison with the experimentally obtained results. The sample is illuminated in the simulation with a TM polarized plane wave propagating in the positive z-direction. The structure is a trench of *450 nm* width and *450 nm* height written in photoresist ($n = 1.5$) that has a. The two small circles denote the position of the phase singularities generated in the transmitted wave-field directly behind the trench. Their distance is directly connected to the width of the structure.

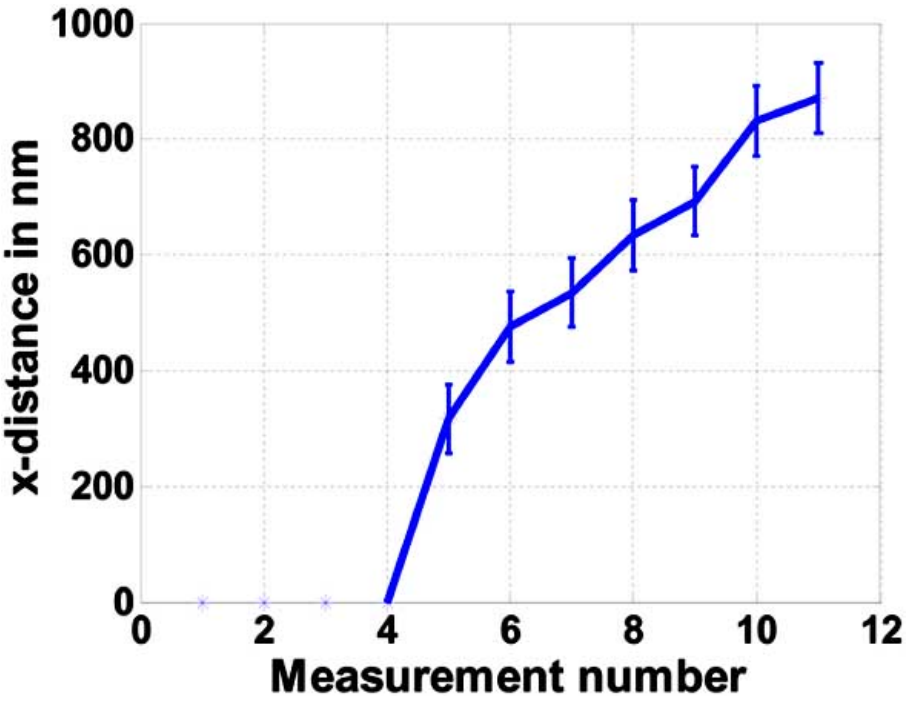

Fig. (12). Measured distance between pairwise generated singularities behind a trench for a series of samples as described in the text.

5.2. Phase Singularities in the Focal Region of Microlenses

Other non-periodic structures that were investigated with the HRIM were microlenses [45]. The field distribution in the focal plane of microlenses is strongly modulated by diffraction due to a high *N.A*. Phase dislocations, such as dark Airy rings, are commonly found near the focal plane, whereas far away from the focus the phase surfaces correspond to spherical wavefronts of geometrical optics [42]. Obtaining three dimensional high-resolution intensity and phase distributions generated by microlenses provides detailed information on important issues for imaging systems. Notably, in integrated optical systems, it is critical to know characteristic parameters such as the focusing quality and optical aberrations of the lens. The form and position of phase dislocations in the focal plane can directly be related to such focal properties and provides excellent criteria for estimation of the quality of the lens system.

For the experimental investigation we used microlenses fabricated by the resist melting technology [43] with a diameter of $d = 30\ \mu m$, a height of $h = 10\ \mu m$ and a focal length of $f \approx 35\ \mu m$ ($N.A. \approx 0.4$). The microlens is illuminated by a plane wave ($\lambda = 488\ nm$) propagating in the z-direction. Three-dimensional measurements are created *via* z-stepping of whole x-y areas using the piezo-stage in the same procedure as described above. Thus, the different cross-sections (x-y, x-z, y-z) can be observed by taking slices through the completed 3D data map. For comparison, rigorous diffraction theory has been used in all cases to calculate the optical fields [26,27]. Only two-dimensional calculations (transverse electric polarization) have been made, because the computational requirements for three-dimensional calculations exceeded by far the available capacities. The measured intensity distribution produced by a microlens along the optical axis (x-z slice) is shown in Fig. **13(a)**. The measured phase distribution is shown in the same figure in (**b**) and (**d**), whereas (c) and (e) show the simulated phases, respectively. Again, in the experimental results the plane $z = 0$ indicates the starting plane of the measurement with no relation to the actual surface of the lens. In the calculated phase distribution, shown in Fig. (**13**) (**c**) and (**e**), the z-axis represents the exact distance to the surface of the microlens. The phase dislocations are marked with circles. For a more obvious representation, the relevant spatial domains are shown magnified in Fig. (**13**) (**d**) and (**e**). The expected strong intensity modulation due to diffraction is clearly present. The measured behavior of the phase in the focal region of the microlens is perfectly reproduced by the simulations. The visible noise in the phase measurements is due to rapid fluctuations in position while scanning and the very low intensity in regions outside the focus. External influences during the measurements are also very critical and can induce relative movements in the phase distribution. On the one hand, we observe the spherical-like wavefronts far from the focus and the microlens. On the other hand, the phase distribution is more turbulent from the focus towards the lens and pairs of phase dislocations or singularities are present in both the measured and calculated fields. The phase singularities always occur in pairs in order to conserve the topology of the optical field. In particular, the first two phase dislocations when approaching the focal region from the far side denote the point where the wavefront curvature changes its direction. In a restricted region between these two dislocations we observe a planar wavefront indicating an effective focus.

In general, dislocations are curved lines in space. In order to visualize the dislocation lines in space the three-dimensional measurement data map is scanned through and the positions of the different pairs of dislocations in each x-z and y-z slice are extracted. Enough singularity positions have been extracted in order to indicate the form of the

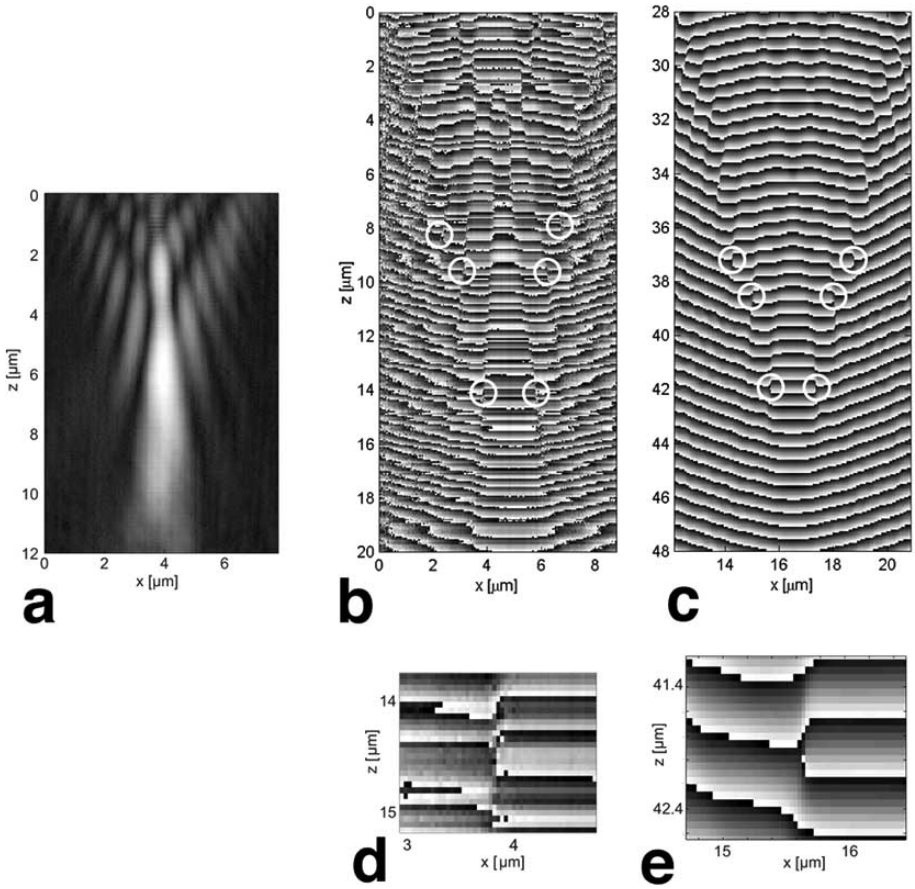

Fig. (13). (**a**) Measured intensity distribution around the focal point of a microlens ($Dz = 50nm$: defined by the step size of the piezo stage, $Dx = 35nm$: pixel size in the object plane) and (**b**) the phase distribution around the focal point of a microlens in as described in the text.

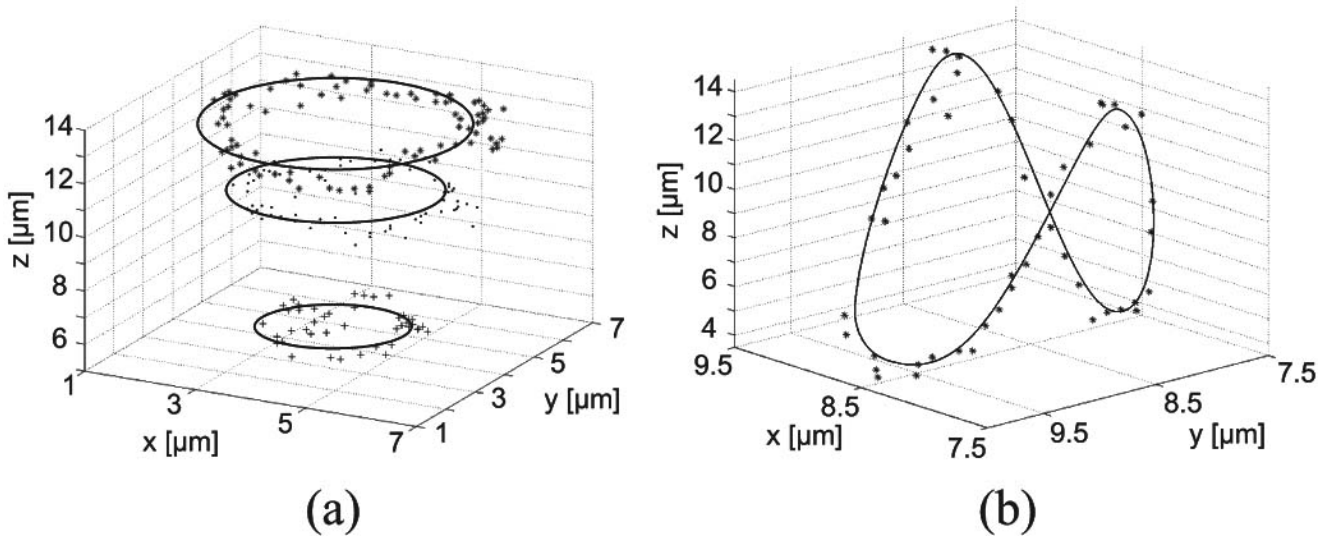

Fig. (14). Phase dislocation positions representing the Airy rings extracted from the 3D measurements of (**a**) a stigmatic microlens and (**b**) an astigmatic lens. Lines have been drawn to guide the eye.

dislocation lines, which are shown for a lens of fairly good quality in Fig. **14(a)**. The phase singularities are situated on different concentric circles forming circle dislocations according the Airy pattern, and because they are perpendicular to the direction of propagation they are of pure edge type [44]. In addition, the fact that the measured dislocations are circles perpendicular to the direction of propagation indicates that the investigated microlens has no serious astigmatic aberrations. In contrast, in the presence of astigmatism, the dislocation circles are distorted out of the plane perpendicular to the optical axis. In Fig. **14(b)**, measurements from a different microlens give an example of such a distorted dislocation. The extracted singularity points forming the dislocation line are no longer situated in a plane perpendicular to the direction of propagation, which indicates astigmatic aberration for the investigated microlens. These three dimensional measurements of microlenses demonstrate that the form and position of the phase dislocations in the focal region is related to imaging properties, such as optical aberrations, which are keyattributes in applications.

CONCLUSIONS AND OUTLOOK

In this mini-review we have presented High-Resolution Interference Microscopy as an experimental tool for measuring the amplitude and phase of electromagnetic waves in the far-field with a spatial resolution down to *20 nm*. We hope that we have been able to familiarize and fascinate the reader with the possibilities of this technique. The instrument was shown to be useful for characterizing screw as well as edge dislocations generated by various periodic and non-periodic objects.

Possible applications for measuring precisely the distance between edge dislocation pairs with the help of the instrument are e.g. in metrology or in an optical data storage system. The application in metrology is evident in the semiconductor industry, as it is mandatory in the fabrication process to structure materials with a precision down to a few tenths of nanometers repetitively. The measurement of the wave-fields scattered by those structure can be used as a non-invasive technique for characterizing the objects *in situ*. The idea for an application in an optical data storage system is somewhat more sophisticated and relies likewise on the precise detection of the distance between the singularities. Information is coded not in a binary scheme but in a multiplexed scheme, wherein different distances can be attributed to specific states of bytes. The information capacity can be significantly increased, as more than a single state can be discriminated within a diffraction limited spot size. In a classical optical data storage system like a CD or DVD, this area of the disc surface can store exactly a single bit. Within this context it was shown by using scalar as well as rigorous diffraction theory, that the size for an object necessary for generating a singularity in the far-field is comparable to the diffraction limit. Although topological features in the wave-field can be discriminated with distances down to a few nanometers, there is no trivial relation to the structural features in the object plane. Rigorous diffraction theory must be used in each case to interpret the measured images properly.

The authors would like to thank Dr. Peter Blattner for initiating the phase singularity work in the optics group at the Institue of Microtechnolgy. In addition we would like to thank Arthur van de Nes from the TU Delft and Andrey Albert Ivanovsky from the National Academy of Sciences of Ukraine for providing us with samples used in some of the measurements. The research was partially supported by the European Union within the framework of the Future and Emerging Technologies-SLAM program under grant No. IST-2000-26479 and the Swiss Priority Program Optique.

REFERENCES

[1] Abbe, E. *Arch. Mikrosk. Anatomie* **1873**, *9*, 413.
[2] Oldenbourg, R. *Nature*, **1996**, *381*, 811.
[3] Ditlbacher, H.; Krenn, J. R.; Lamprecht, B.; Leitner, A.; Aussenegg, F. R. *Opt. Lett.,* **2000,** *25*, 563.
[4] Hellwarth, R.; Christensen, P. *Appl. Opt.*, **1975**, *14*, 247.

[5] Pohl, D. W.; Courjon, D. *Near Field Optics*, Kluwer: Dordrecht, **1993**.

[6] Kawata, S.; Inouye, Y.; Sugiura, T. *Jpn. J. Appl. Phys.*, **1994,** *33*, *L*1725.

[7] Zernicke, F. *Science*, **1995**, *121*, 345.

[8] Nye, J. F.; Berry, M. V. *Proc. Roy. Soc. Lond. A,* **1979**, *336*, 165.

[9] Basisty, I.V.; Bazhenov, V.Yu.; Soskin, M.S.; Vasnetsov, M.V. *Opt. Commun.*, **1996**, *103*, 422.

[10] Nye, J. F. *J. Opt. Soc. Am. A,*, **1998**, *15*, 1132.

[11] Siegman, A. E. *Lasers*, University Science Books, Mill Valey, California, **1986**.

[12] Baranova, N. B.; Mamaev, A. V.; Polopetsky, N. F.; Shkunov, V. V.; Zel'dovich, B. Y. *JETP Lett.*, **1981**, *33*, 195.

[13] Freund, I.; Shvartsman, N.; Freilikher, V. *Opt. Commun.*, **1993**, 101, 247.

[14] Harris, M.; Hill, C. A.; Vaughan, J. M. *Opt. Commun.*, **1994**, *106*, 161.

[15] Beijersbergen, M. W.; Coerwinkel, R. P. C. ; Kristensen, M.; Woerdman, J. P. *Opt. Commun.*, **1992**, *112*, 321.

[16] Machavariani, G.; Davidson, N. ; Hasman, E.; Blit, S.; Ishaaya, A. A.; Friesem, A. A. *Opt. Commun.*, **2002**, *209*, 265.

[17] Petrov, D. V.; Canal, F.; Torner, L. *Opt. Commun.*, **1997**, *143*, 265.

[18] Rozas, D.; Sacks, Z. S.; Swartzlander, Jr., G. A. *Phys. Rev. Lett.*, **1997**, *79*, 3399.

[19] Heckenberg, N. R.; McDuff, R. ; Smith, C. P.; White, A. G. *Opt. Lett.*, **1992**, *17*, 221.

[20] Grier, D. G. *Nature*, **2003**, *424*, 810.

[21] Kuga, T. ; Torii, Y.; Shiokawa, N.; Hirano. T. *Phys. Rev. Lett.*, **1997**, *78*, 4713.

[22] Tychinsky, V.P. *Opt. Commun.*, **1989**, *74*, 41 .

[23] Tychinsky, V. P. ; Masalov, I. N.; Pankov, V. P.; Ublinsky, D. V. *Opt. Commun.*, **1989**, *74,* 37 .

[24] Tychinsky V. P.; Velzel, C. H. F. In *Current Trends in Optics*, Dainty, J. C., Ed.; Academic Press London, **1994**, pp. 255–268.

[25] Rockstuhl, C.; Salt, M.; Herzig, H. P. *Opt. Commun.*, **2004**, *235*, 11.

[26] Turunen, J. in *Micro-Optics: Elements, Systems and Applications*, Herzig, H. P., Ed.; Taylor & Francis, **1997**.

[27] Moharam, M.G.; Gaylord, T.K. *J. Opt. Soc. Am.*, **1981**, *72,* 1385.

[28] Blattner, P.; Herzig, H.P. *J. Mod. Opt.*, **1998**, *45*, 1395 .

[29] Totzeck, M.; Krumbügel, M.A. *Opt. Commun.,* **1994**, *112*, 189.

[30] Krumbügel, M.A.; Totzeck, M. *Opt. Commun.*, **1993**, *98*, 47.

[31] Eberler, M.; Dorn, R.; Münzer, B.; Quabis, S.; Leuchs, G. *In Proceedings of the World Conference on Systematics*, Cybernetics and Informatics, Orlando, **2000**.

[32] Schouten, H.F.; Gbur, G.; Visser, T.D.; Lenstra, D.; Blok, H. *Opt. Express,* **2003**, *11*, 371.

[33] Rockstuhl, C.; Salt, M.; Herzig, H. P. *J. Opt. A: Pure Appl. Opt.*, **2004**, *6*, S271.

[34] Schwider, J.; Burow, R.; Elssner, K. E.; Grzanna, J.; Spolaczyk, R.; Merkel, K. *Appl. Opt.*, **1983**, *22*, 3421.

[35] Dändliker, R.; Blattner, P.; Rockstuhl, C.; Herzig, H. P. In *Singular optics (optical vortices): fundamentals and applications*, SPIE Proc., **2000**, *4403*, pp. 257–261.

[36] Rockstuhl, C.; Ivanovskyy, A. A.; Soskin, M. S.; Salt, M.; Herzig, H. P.; Dändliker, R. *Opt. Commun.*, **2004**, *242*, 163.

[37] Basistiy, I.V.; Soskin, M.S.; Vasnetsov, M.V. *Opt. Commun.*, **1996**, *119*, 604.

[38] Ivanovskyy, A. A.; Basistiy, I. V.; Soskin, M. S. *Semiconduct Phys. Quantum Electron. J.*, **2003**, *6*, 249.

[39] Angelsky, O. V.; Mokhun, I. I.; Mokhun, A. I.; Soskin, M. S. *Phys. Rev. B*, **2002**, *65*, 036602.

[40] Blattner, P. *Light fields emerging from periodic optical microstructures*, PhD dissertation, University Neuchâtel, Switzerland **1998**.

[41] Totzeck, M.; Jacobsen, H.; Tiziani, H. J. *SPIE Proc.*, **1999**, *3897*, pp. 424–435.

[42] Born, M. and Wolf E., *Principles of Optics*, Cambridge University Press, Cambridge, UK, **1999**.

[43] Hutley M. C. In *Micro-Optics: Elements, Systems and Applications*, Herzig, H. P., Ed.; Taylor & Francis, **1997**.

[44] Nye, J. F. *Natural Focusing and Fine Structure of Light, Caustics and Wave Dislocations*, Bristol: Institute of Physics Publishing, **1999**.

[45] Dändliker, R., Märki, I., Salt, M., Nsci, A., *J. Opt. A.: Pure Appl. Opt.,* **2004**, *6*, pp. 5189-5196.